

Active Suspension Vibration Control with Dual Stage Actuators in Hard Disk Drives¹

Yunfeng Li and Roberto Horowitz

Computer Mechanics Laboratory (CML)

Department of Mechanical Engineering

University of California at Berkeley, CA 94720-1740

yunfeng@me.berkeley.edu, horowitz@me.berkeley.edu

Abstract

This paper discusses the design of adaptive feedforward control for dual stage servo system in disk drives, which utilizes vibration signal obtained from instrumented suspension, in order to compensate track mis-registration (TMR) due to air flow excited suspension vibration. Experiments are conducted on a spin stand to evaluate the TMR due to air flow excited suspension vibration using LDV. Adaptive feedforward control is designed to cancel suspension vibration, by using the strain signal on the surface of the instrumented suspension, and controlling slider with a MEMS microactuator (MA). An off-line MA model identification method, which does not utilize relative position sensing is also proposed. Simulations show the proposed technique can successfully suppress the suspension vibration induced TMR.

1 Introduction

It is expected that most of the track mis-Registration (TMR) due to track runout and low frequency disturbances in hard disk drives can be greatly attenuated by extending the bandwidth of the track following servo using dual stage actuation. However, it is also expected that, with increased spindle rotation speed, air flow induced suspension vibration will become a major obstacle to achieve higher track density for dual stage servos. The structural resonance modes of the suspension are generally located at a higher frequency than the predicted servo bandwidth, which is limited by the position error signal (PES) sampling rate. Thus, the TMR due to suspension vibration can not be sufficiently attenuated with only PES feedback control. In fact, the suspension vibration can be amplified by the feedback controller.

The idea of using strain sensors to control the actuator vibration modes has been proposed to increase the bandwidth

of single stage servos using only a voice coil motor (VCM) actuator [1], [2]. In [1], it is proposed to attach strain gauges at proper locations on the suspension to control the suspension vibration modes. In [2], strain sensors are attached to the E-block to damp its butterfly resonance mode. In this paper, we discuss active suspension vibration compensation with dual stage servo using similar techniques.

There are two strategies for suspension vibration control using dual stage servo systems, depending on the configuration and location of the microactuators (MA). For a PZT actuated suspension dual stage system, the actuation is behind the suspension vibration modes. A feedback active damping control scheme similar to the ones described in [1] and [2], can be utilized to damp the resonance modes. The only difference is that now the strain feedback control can be applied to the PZT MA instead of the VCM, as in the single stage case. This paper is mainly focused on suspension vibration compensation for an actuated slider dual stage servo system, which utilizes a MEMS MA positioned at the end of the suspension. In this case, the actuation is in front of the suspension. Adaptive feedforward control can be used so that motion of the MA cancels the TMR induced by the suspension vibration.

This paper is organized as follows: section 2 discusses the testing of air flow induced suspension vibration. In section 3, the configuration of a dual stage actuation with an instrumented suspension is first briefly introduced. Next, we present the formulation of an adaptive feedforward controller, and a MA model identification technique that is needed for the adaptation algorithm. Simulation results of dual stage feedback control combined with adaptive feedforward control is provided in section 4. Section 5 contains conclusions and discussions of future work.

2 Air Flow Induced Suspension Vibration

With increasing spindle rotation speed, the air flow excitation impinging on the actuator arm is becoming a very important factor affecting TMR. To study the suspension vibra-

¹Research supported by the National Storage Industry Consortium (NSIC) and the Computer Mechanics Laboratory (CML) of U.C. Berkeley.

tion due to air flow excitation, experiments were conducted with a fixed single suspension mounted on a spin stand, as shown in Fig. 1. The lateral motion of the slider was measured with a Laser Doppler Vibrometer (LDV) when it is flying on a 3.5" disk.

Fig. 2 shows the averaged FFT of the displacement of the slider for spindle rotational speed of 7200, 10k and 15k RPM respectively. The measurement is taken at the outside diameter of the disk, which has a radius of 40mm.

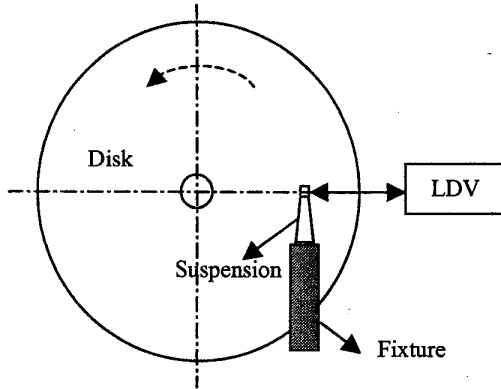


Figure 1: Suspension vibration measurement setup

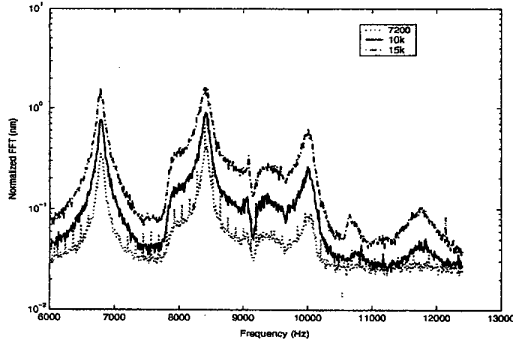


Figure 2: FFT of slider motion due to air flow induced suspension vibration

The spectrum shown in Fig. 2 matches the suspension vibration modes obtained using finite element analysis (FEA). The resonance peak at 6.8 kHz corresponds to the suspension's 1st torsional mode (6.7 kHz by FEA), and the peak at 8.4 kHz corresponds to the sway mode (8.6 kHz by FEA). Thus, air flow affects TMR mainly by exciting the suspension's own resonance modes. This observation points toward the possibility of using the strain signal on the surface of the suspension for control, in order to suppress air flow induced TMR.

We also found the power spectrum of the motion of the slider due to air flow induced suspension vibration changes with respect to the location of the suspension on the disk. For example, the torsional mode becomes smaller at the inside diameter of the disk.

Because of the drift in the LDV output and the existence of fixture resonance modes in 2-3 kHz range, we were not able to calculate the TMR directly using the time domain observation. However, we can estimate the TMR due to air flow induced suspension vibration using the power spectrum in the interested frequency range, by the following formula,

$$\sigma = \sqrt{E[x^2(i)]} = \sqrt{\sum_{i=n_1}^{n_2} |X(i)|^2}, \quad (1)$$

where $x(i)$ is the motion of the slider due to suspension vibration, $X(i)$ is the normalized FFT, and n_1 to n_2 specifies the frequency range. TMR was estimated using Eq. (1) by summing the power spectrum from 6 kHz to 12.4 kHz, and the results are listed in the following table:

Rotation Speed (RPM)	7200	10,000	15,000
Estimated σ (nm)	3.6	5.8	9.4

Note: the TMR budget (σ value) for 100k tracks per inch (TPI) is about 8 nm.

We can see that the spindle rotation speed has a big impact on the air flow induced suspension vibration. Moreover, suspension vibration may become a very important obstacle to achieve very high track densities for high RPM disk drives if it is not properly compensated. However, due to PES sampling frequency limitations, it cannot be sufficiently suppressed solely by PES feedback control, and in fact it may be amplified.

Bode's Integral Theorem states that the integral of the magnitude of the closed loop sensitivity transfer function (TF) is a constant regardless of the chosen controller [3]. A typical magnitude plot of the sensitivity TF from runout to PES is shown in Fig. 3. Note that suspension vibration can be taken as an external runout to the feedback system. At low frequency, the sensitivity TF attenuates the runout. However, it amplifies the runout beyond its unity gain frequency, which is approximately equal to the bandwidth of the feedback system.

Dual stage servo systems can achieve a higher bandwidth than conventional single stage systems, and consequently bigger low frequency attenuation. Thus, track runout and other low frequency disturbances can be greatly attenuated. However, the bandwidth of dual stage servo is still limited by the PES sampling frequency, which in turn is limited by data storage efficiency. For example, the achievable bandwidth for a 40 kHz PES sampling frequency is about 5 kHz. The power spectrum in Fig. 2 shows that suspension vibration has big components in the 6-12 kHz range. According to the Bode's Integral Theorem, the PES due to these vi-

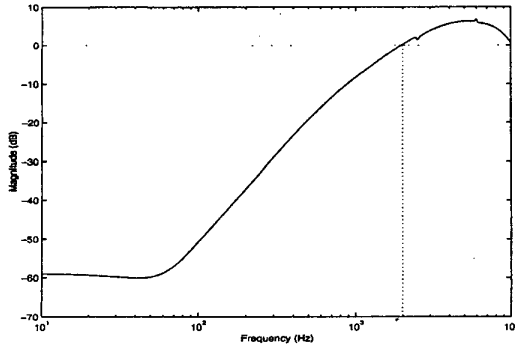


Figure 3: Magnitude plot of sensitivity transfer function

bration modes can be amplified by the dual stage feedback control system.

To solve this problem, we propose to utilize additional sensors to measure the suspension vibration, which can have a faster sampling rate than of the PES, and either use active feedback damping control or feedforward cancellation technique with dual stage actuators to compensate the suspension vibration induced TMR.

3 Adaptive Vibration Cancellation with Dual Stage Servo and Instrumented Suspension

3.1 Dual Stage Servos with Instrumented Suspensions

Strain sensors can be attached or fabricated onto the surface of a suspension to measure its vibration. A Piezoresistor strain sensors are good candidate because of its big gauge factor, and the possibility of integrating its fabrication with that of the suspension using microfabrication techniques. Such a sensor has been successfully fabricated on a silicon suspension as relative position sensor [4]. Potentially it also can be incorporated on a metal suspension to act as vibration modes sensor.

The location and orientation of the sensor will be optimized to give the biggest correlation between the strain sensor output and the off-track motion of the slider due to suspension vibration. A method to search the optimal sensor location and orientation on the load beam has been proposed in [1]. Using this method, a state space realization of the strain sensor output and the vibration modes is established using FEA. The optimal location and orientation of the strain sensor is determined by maximizing of the smallest singular value of the observability grammian of the state space system.

Different schemes for suspension vibration control are needed, depending on the type and configuration of the dual stage servo system. For PZT actuated suspension dual stage servo systems, where the PZT actuator is located in front of the suspension, feedback active damping control can be

applied. For MEMS-based actuated slider dual stage servo systems, the piggy-back MA is located at the tip of the suspension and it has little effect on the suspension dynamics. In this case, feedforward control can be used to cancel the TMR induced by suspension vibration.

3.2 Adaptive Feedforward Suspension Vibration Compensation

An adaptive feedforward control structure for vibration cancellation is shown in Fig. 4. For simplicity, dual stage feedback part is not included.

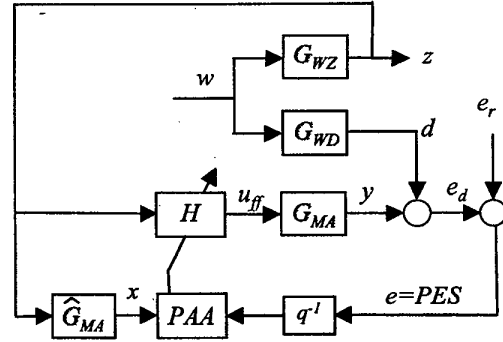


Figure 4: Adaptive feedforward control for vibration cancellation

In the figure, w represents the air flow excitation to the suspension. d is the head motion due to suspension vibration, G_{wd} is the TF from w to d , z is the strain sensor output, and G_{wz} is the TF from w to z . Ideally we would like z and d to have biggest possible correlation. However, since z and d represent the effects of vibration at different locations in the suspension, even though the poles of G_{wz} and G_{wd} may be the same, they usually have different zeros, and therefore, d and z will probably have a dynamic relationship. We define the TF from z to d to be

$$G_{zd} = \frac{G_{wd}}{G_{wz}} \quad (2)$$

G_{MA} in Fig. 4 is the TF of the MA. H is the feedforward filter, which needs to be designed, in order to cancel d . Intuitively, an expression for H can be

$$H = (G_{MA})^{-1} G_{zd} \quad (3)$$

However, H as given by Eq. (3) may not be causal and the transfer functions of G_{zd} is not precisely known. Furthermore, the strain gauge factor usually is sensitive to the temperature. Thus, the optimal filter H needs to be estimated using an adaptive scheme. In our approach, H is approximated with a finite impulse response (FIR) filter for stability considerations. It can be written as

$$H(q^{-1}) = h_0 + h_1 q^{-1} + \dots + h_M^{-M} \quad (4)$$

where q^{-1} is the one step delay operator and M is the order of the FIR filter. The output of the MA is

$$\begin{aligned} y(k) &= G_{MA}(q^{-1})u_{ff} \\ &= G_{MA}(q^{-1})H(q^{-1})z(k) \\ &= H(q^{-1})G_{MA}(q^{-1})z(k). \end{aligned} \quad (5)$$

Let

$$x(k) = G_{MA}(q^{-1})z(k), \quad (6)$$

and define the regressor vector,

$$\phi(k) = [x(k) \ x(k-1) \ \dots \ x(k-M)]^T, \quad (7)$$

and the FIR tap weight vector,

$$\theta = [h_0 \ h_1 \ \dots \ h_M]^T. \quad (8)$$

The output equation of the MA can be written as

$$y(k) = \theta^T \phi(k). \quad (9)$$

And the vibration compensation error is

$$e_d(k) = y(k) + d(k). \quad (10)$$

Parameter adaptation algorithm (PAA) can be used to estimate the coefficients of $H(q^{-1})$, $\hat{\theta}$, to minimize the mean square value of e_d , $E[|e_d(k)|^2]$. However, e_d is not available, and the error signal we have access to is the PES, which can be written as

$$e(k) = e_d(k) + e_r(k), \quad (11)$$

where e_r represents the position error from other sources, such as runout, after compensated by the feedback controller. Assuming that d is uncorrelated with e_r , we have

$$E[|e(k)|^2] = E[|e_d(k)|^2] + E[|e_r(k)|^2]. \quad (12)$$

Thus, minimizing $E[|e(k)|^2]$ is equivalent to minimize $E[|e_d(k)|^2]$. Thus, we can use the PES, e , as a corrupted error signal to do the adaptation, where e_r acts as the measurement noise for the adaptation process.

The regressor defined in Eq. (6) will be estimated by filtering z with the MA model, \hat{G}_{MA} .

$$\hat{x}(k) = \hat{G}_{MA}(q^{-1})z(k). \quad (13)$$

In next section, we will discuss how \hat{G}_{MA} is obtained.

The recursive least square (RLS) PAA for tuning the tap weights of H is [6]

$$\hat{\theta}(k) = \hat{\theta}(k-1) + P(k)\phi(k)e(k-1), \quad (14)$$

$$\begin{aligned} P(k) &= P(k-1) \\ &- \frac{P(k-1)\phi(k-1)\phi^T(k-1)P(k-1)}{1 + \phi^T(k-1)P(k-1)\phi(k-1)} \end{aligned} \quad (15)$$

Other simplified algorithms, such as the LMS algorithm, also can be used.

3.3 MA Model Identification

The dynamics of a typical MEMS MA can be accurately described by a second order linear system model, without appreciable high order dynamics up to 40 kHz [5]. However, due to lithographic misalignment and variations present in the etching processes, the resonance frequency of the MA, which has a nominal value of 1.5 kHz, can vary by as much as $\pm 15\%$ from its designed nominal value from one MA to another. It is possible to incorporate an additional PAA to the control system described in the block diagram in Fig. 4 to identify the MA model in real time [7]. However, since the variations in the MA's resonance frequency usually does not change after it has been fabricated, we can use an off-line scheme to identify the MA model before hand.

The MA model can be described with a second order mass-spring-damper system model. The discrete time TF of the MA model can be written as

$$G_{MA}(q^{-1}) = \frac{q^{-1}B_o(q^{-1})}{A_o(q^{-1})}, \quad (16)$$

where $B_o(q^{-1})$ and $A_o(q^{-1})$ are respectively the MA open loop zero and pole polynomials:

$$B_o(q^{-1}) = b_0 + b_1q^{-1}, \quad (17)$$

$$A_o(q^{-1}) = 1 + a_1q^{-1} + a_2q^{-2}. \quad (18)$$

Let the relative position error signal (*RPES*) represents the position of the MA relative to the tip of suspension. Based on the availability of an *RPES* sensor, different methods can be used to identify the MA model. When the *RPES* is available. The open loop MA dynamics can be identified by feeding to the MA a white excitation input signal. The model parameters identification is based on the model

$$A_o(q^{-1})y(k) = q^{-1}B_o(q^{-1})u_M(k) + w(k), \quad (19)$$

where $u_M(k)$ is the input excitation signal to the MA, $y(k)$ is the *RPES* and $w(k)$ is the *RPES* measurement noise.

When the *RPES* sensor is not available and the only available feedback signal to the control system is the *PES*, it is still possible to identify the MA open loop dynamics by closing the VCM loop with the *PES*, and feeding an excitation input signal of a sufficiently large magnitude to the MA, as shown in Fig. 5.

Defining this time $y(k)$ to be the *PES*, we have

$$y(k) = r(k) - G_{MA}u_M(k) - K_V G_V y(k), \quad (20)$$

where r represents the runout, $u_M(k)$ is the input excitation signal to the MA, G_{MA} and G_V are respectively the TFs of the MA and the VCM. Define the closed loop sensitivity TF of the VCM,

$$S_V = \frac{1}{1 + K_V G_V}. \quad (21)$$

and define the filtered excitation to the MA by

$$u_M^f(k) = -S_V u_M(k), \quad (22)$$

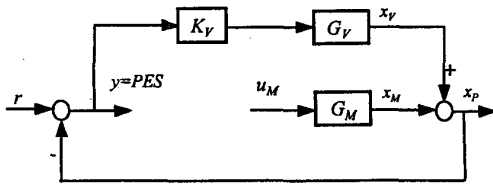


Figure 5: MA model identification with no RPES sensing

we obtain,

$$y(k) = G_{MA} u_M^f(k) + S_V r(k), \quad (23)$$

In the above equation, the term $S_V r(k)$ represent the PES due to the runout after it has been rejected by the VCM sensitivity TF. It is small as compared to the PES due to the excitation of the MA, since we choose u_M to be sufficiently large. Eq. (23) can be re-written as

$$A_o(q^{-1})y(k) = q^{-1}B_o(q^{-1})u_M^f(k) + C(q^{-1})w(k), \quad (24)$$

where A_o , B_o are the MA open loop pole and zero polynomials, which need to be identified, $w(k)$ is a fictitious white noise, and the $C(q^{-1})$ represents the combined effect of runout, VCM and MA torque disturbances, and the PES measurement noise, after being rejected by the VCM controller.

Fig. 6 shows the simulated response of the MA parameters estimates \hat{a}_1 , \hat{a}_2 , \hat{b}_o , \hat{b}_1 , using the extended recursive least square (ERLS) algorithm [6]. In the simulation, realistic estimates of the runout, VCM and MA torque disturbances, PES measurement noise are injected into the dual stage system at corresponding locations. u_M was a white excitation with a sufficient large amplitude to generate about $\pm 1 \mu\text{m}$ of MA motion and $\hat{C}(q^{-1})$ was chosen to be fourth order. As shown in Fig. 6, the parameters estimates converged to their true values.

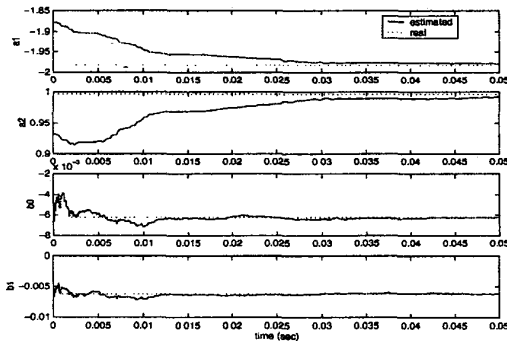


Figure 6: Control parameters adaptation responses

4 Simulation Results

Simulations were conducted using a MEMS MA dual stage model. The dual stage feedback controller was designed using the sensitivity decoupling method described in [7]. The sampling frequency was assumed to be 40 kHz. The designed dual stage feedback controller has an open loop cross-over frequency of 4.6 kHz. The Bode plot of G_{wd} , G_{wz} used in the simulation are shown in Fig. 7. Notice, they have the same poles, but slightly different zeros.

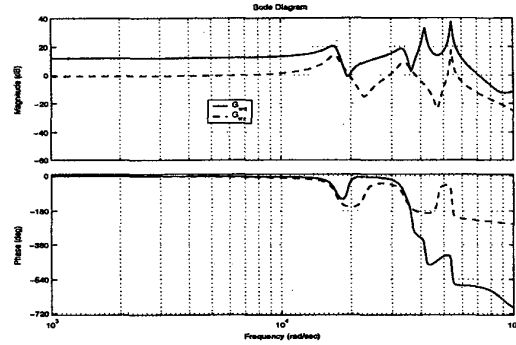


Figure 7: Bode plot of G_{wd} and G_{wz}

Runout, disturbances, and measurement noises are injected into the plant at corresponding locations. Fig. 8 shows the FFT of the PES when feedforward vibration cancellation is not applied. The standard deviation of the PES is $\sigma_{PES} = 15.3 \text{ nm}$. As shown in the figure, track runout and low frequency disturbances have been greatly attenuated by the high bandwidth feedback controller. However, there are peaks in the 6-12 kHz range, which are due to air flow excited suspension vibration.

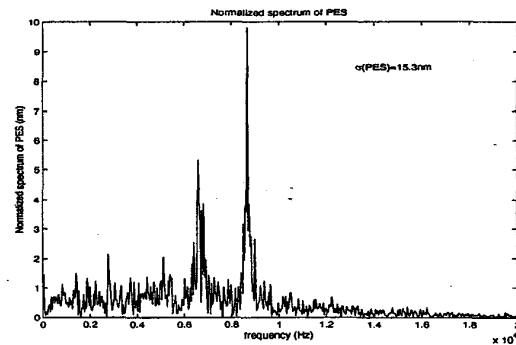


Figure 8: FFT of PES without feedforward control

Fig. 9 shows the FFT of the PES when adaptive feedforward control is applied, and after the control parameters have converged. The FIR filter is chosen to be 6-tap.

We can see that the adaptive feedforward controller for the MA can successfully compensate the suspension vibration rounout, as evidenced by the significant reduction in the magnitude of the FFT peaks in the 6-12 kHz range. In this case, $\sigma_{PES} = 9.4 \text{ nm}$, and better performance can be achieved with a higher order FIR.

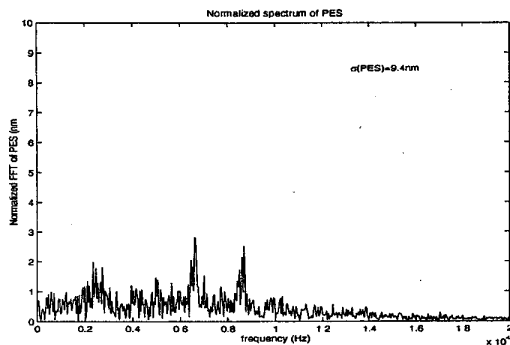


Figure 9: FFT of PES with adaptive feedforward control

Fig. 10 shows the simulated adaptation process of the FIR filter tap weights. Notice that the adaptation convergence is slow (it takes about 20ms for the tap weights to converge). However, this can be improved by using an algorithm similar to the one developed in [8] by incorporating an additional plant and noise model identification PAA. Alternatively, we can use an off-line pre-tuning process to establish a table of the optimal feedforward filter coefficients with respect to different locations on the disk. The feedforward filter then can be fine tuned in real time.

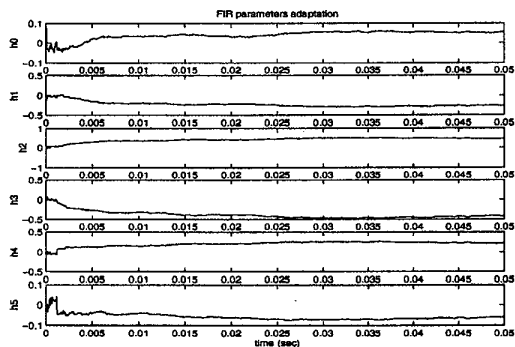


Figure 10: FIR tap weights adaptation

5 Conclusion and Future Work

Suspension vibration induced TMR poses a significant challenge for servo design to achieve very high track density in high RPM disk drives. By incorporating additional

vibration sensors with instrumented suspension, suspension vibration can be compensated with dual stage actuators. An adaptive feedforward control scheme was developed to cancel the suspension vibration for actuated slider dual stage system.

Future work related to this paper includes, the deign and fabrication of the vibration sensors using piezo-resistors, formulation of the multi-rate adaptation scheme with feed-forward loop running at a faster rate than the adaptation loop, and experimental validation of the proposed vibration compensation scheme.

References

- [1] Y. Huang, M. Banther, P.D. Mathur, W.C. Messner, "Design and Analysis of a High Bandwidth Disk Drive Servo System Using an Instrumented Suspension", *IEEE/ASME transaction of Mechatronics, Vol. 4, No. 2, June 1999*.
- [2] F.-Y. Huang, W. Imano, T. Semba, F. Lee, "Rotary Actuator Dynamics with Active Damping", *11th Annual Symposium on Information Storage and Processing System, June, 2000*
- [3] C. Mohtadi, MA, DPhil, "Bode's Integral Theorem for Discrete-time System", *IEE Proceedings D, vol.137, March 1990*
- [4] T. Chen, R. Horowitz, "Design, Fabrication and Dynamic Analysis of a PZT-actuated Silicon Suspension", *Proceedings of American Automatic Control Conference, June, 2001*
- [5] L.-S. Fan, T. Hirano, J. Hong, P. R. Webb, W.H. Juan, W. Y. Lee, S. Chan, T. Semba, W. Imano, T.S. Pan, S. Patanaik, F.C. Lee, I. McFadyen, S. Arya, R. Wood, "Electrostatic microactuator and design considerations for hdd application", *IEEE Transactions on Magnetics, vol. 35, no. 2, March 1999*.
- [6] K. J. Åström, B. Wittenmark, *Computer Controlled Systems: Theory and Design*, Prentice-Hall, 1984.
- [7] Y. Li, R. Horowitz, "Analysis and Self-tuning Control of Dual Stage Servos with MEMS Micro-actuators", *Proceedings of American Automatic Control Conference, June, 2000*
- [8] S. Pannu, R. Horowitz, "Increased Disturbance Rejection for Hard Disk Drives Using Accelerometers", *The Journal of Information Storage and Processing Systems, Vol. 1, 1999*